EDGE ARTICLE

CrossMark
click for updates

The ligand unwrapping/rewrapping pathway that exchanges metals in S-acetylated, hexacoordinate N₂S₂O₂ complexes†

J. A. Denny, W. S. Foley, A. D. Todd and M. Y. Darensbourg*

The effect of S-acetylation in MN_2S_2 complexes on metal exchange reactivity was examined in a series of $MN_2S_2O_2$ complexes. While clean exchange processes do not occur for the MN_2S_2 derivatives where formation of S-bridged aggregates predominate, acetylation permits the metal exchange with hierarchy that follows the Irving–Williams series of stability for first row transition metals: $Fe^{2+} < Co^{2+} < Ni^{2+} < Cu^{2+} > Zn^{2+}$. The rate determining step consistent with kinetic parameters depends on both M and M′, supporting a mechanism of exchange that involves ligand unwrapping/rewrapping process as earlier defined by Margerum *et al.* for M(EDTA) systems. The enhanced metal exchange deriving from S-acetylation is of significance to probes and detection of cysteine-S metallo-proteins and metallo-enzyme active sites, and highlights a new role for S-acetylation.

Introduction

For the coordination chemist, there are no "free" metal ions. In solution, all synthetic procedures entail the transfer of metal ions from one binding site to another, usually involving intricate mechanisms of stepwise and cascading de- and re-ligation.[1] An analogue of this process of particular interest to bio-inorganic chemistry lies in the construction of catalytic sites of metalloenzymes involving nitrogen and sulfur donor atoms from protein-bound histidine imidazoles, cysteine thiolates, methionine thioethers, and tripeptide motifs with deprotonated amido nitrogens.[2–4] In the form of a protein–Cys–X–Cys–protein chain, such a motif results in a contiguous, largely square planar S–N–N–S tight binding site, displayed in the distal nickel site of acetyl-CoA-synthase (ACS),[5] the cobalt site of thiocyanate hydratase,[6] and in the iron and cobalt forms of nitrile hydratase (NHase),[7] Fig. 1. The sulfurs of the Cys–Ser–Cys tripeptide binding motif found in Co- and Fe-NHase are "post-translationally modified" with oxygen, yielding metallosulfinyl (R–S=O) and metallosulfonato (R–S(=O)₂) units.[8] Similar sulfur reactivity is characteristic of synthetic N₂S₂ complexes of nickel, where the N₂S₂ binding is maintained throughout a variety of nickel-bound S-modifications; including metallation, oxygenation, and simple alkylation, Fig. 2.[9–13]

Department of Chemistry, Texas A&M University, College Station, Texas 77843, USA. E-mail: marcetta@chem.tamu.edu

The reactivity of cysteinyl sulfur in proteins with acetylating agents, such as iodoacetamide, AA, and iodoacetate, Ac, has found application for cysteine protection and as an analytical tool for protein sequencing/mass spectrometry experiments.[14–19] The latter is used to monitor the increased mass of the cysteine residues and of the protein as a whole, and in the former, to prevent the formation of disulfide bonds in the tertiary structure of proteins.[20] While thioethers are typically poorer metal-binding ligands, the carboxylate or carboxamido terminus is a potential donor, leading to the possibility of coordination number expansion.[21] It is generally expected that alkylation of cysteines in an apo-active site can prevent the coordination of metal(s); alternatively, alkylation on sulfurs of metal-bound cysteines may deactivate the enzyme.[15,16] As alkylating and acetylating agents are known carcinogens, knowledge of potential sites of reactivity in biomolecules is of even greater significance.

The work described herein was initiated in response to a need to understand the properties of zinc in N₂S₂ binding
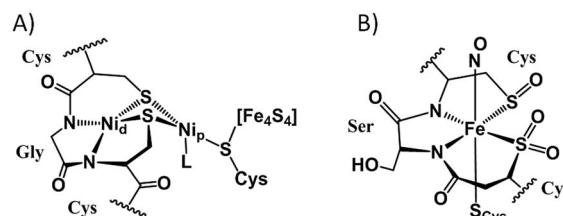

Fig. 1 Cys–X–Cys N₂S₂-containing active sites of enzymes with S-modification: (A) the nickelated sulfurs in acetyl-CoA synthase;[5] Ni_p designates the nickel proximal to the 4Fe4S cluster while Ni_d is distal. (B) The O-atom S-modified site in the as-isolated iron form of nitrile hydratase.[7]

Fig. 2 Synthetic MN$_2$S$_2$ complexes showing modification of thiolates by oxygenation, alkylation, or metallation.

Fig. 3 Scheme for the synthesis of **Ni-1'-Ac$_2$** and **Zn-1'-Ac$_{1/2}$** in MeOH, adapted from ref. 30 and 31.

environments and its response to extraneous metals. As the second most abundant transition metal in the human body, zinc is most commonly found as a structural element. The exchange of Zn^{2+} by Pt^{2+} in zinc finger sites on transcription factors is theorized to be part of the mechanism by which *cis*-platin can interrupt DNA replication in cells.[22] Zinc is a catalytic center in enzymes such as carbonic anhydrase, and carboxy-peptidase where exchange with metal ions that have useful spectroscopic features has proven useful to define the roles of the spectroscopically silent zinc.[23–25] In metallothionein proteins its kinetic lability may be exploited in exchanges with toxic metals. It may act as a place-holder in a preformed apo-enzyme active site,[26] for example, HypB in the maturation cycle of NiFe-hydrogenase.[27,28] In abiological areas, Escudero-Adan *et al.* have used transmetallation of Zn–salphen complexes as a synthetic approach to a library of transition metal salphen complexes.[29]

In addition to the significance of metal exchange processes described above, chelation therapy and/or toxic metal removal has inspired extensive studies of the transmetallation of Ni(EDTA)$^{2-}$ with Cu^{2+} by Margerum, *et al.* where kinetic data served as basis for a proposed mechanism.[1,30] The likely simi-larity of the functional carboxylate exterior of the EDTA complexes and the acetylated N$_2$S$_2$ complexes has guided interpretation of the kinetic studies described below.

Fig. 3 summarizes our earlier synthesis and reactivity studies that showed acetylation of metal-bound thiolates in zinc and nickel complexes containing the tight N$_2$S$_2$ binding site, con-verting the thiolate sulfurs into thioethers, concomitant with expansion of ligand denticity through the carboxylate group, *i.e.*, resulting in MN$_2$S$_2$O$_2$ formulation.[31,32] The thus derived thioethers maintained binding to the metal with notable differences in chemical properties between the unmodified **M-1'** complexes and their counterparts, **M-1'-Ac$_2$**, Fig. 3. Herein we advance such *S*-acetylations, yielding a series of six-coordinate complexes that have been characterized for comparison to the products of metal exchange reactions between **M-1'-Ac$_2$** complexes and exogenous metal ions. Despite their coordina-tive saturation within a hexadentate ligand, the **M-1'-Ac$_2$** complexes readily undergo transmetallation. Kinetic studies indicate a bimolecular process, presumably involving a ligand unwrapping/wrapping mechanism similar to what was proposed for metal exchange in the EDTA complexes and their derivatives.[1,30,33–35]
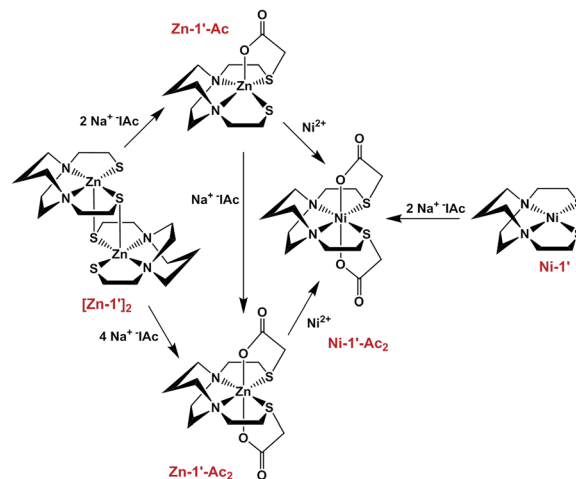
Results and discussion

Templated synthesis of M-1'-Ac$_2$

Similar to the preparation of diacetylated Ni(bme-daco), **Ni-1-Ac$_2$**,[32] an excess of Na$^+$[ICH$_2$CO$_2$]$^-$ reacts with the thiolate sulfurs of the parent **[M-1']$_2$** complexes in methanol to yield the **Co-1'-Ac$_2$** and **Fe-1'-Ac$_2$** complexes, isolated in 98% and 72% yields, respectively, route (a), Fig. 4.

Metallation of the sodium salt of the hexadentate ligand Na$_2$-1'-Ac$_2$ to form M-1'-Ac$_2$

The hexadentate ligand **Na$_2$-1'-Ac$_2$** was synthesized as previously reported through the reaction of a slight excess of Na$^+$[ICH$_2$-CO$_2$]$^-$ with the H$_2$bme-dach ligand in MeOH, Fig. 4.[36] The products isolated from addition of Co(NO$_3$)$_2$ and Fe(NO$_3$)$_2$ route (b), Fig. 4, had physical properties matching the **M-1'-Ac$_2$**
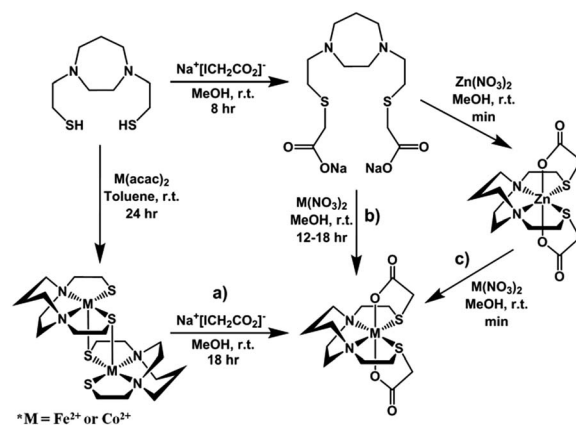

Fig. 4 Synthetic routes yielding **M-1'-Ac$_2$** complexes: (a) templated synthesis from acetylation of [MN$_2$S$_2$]$_2$ precursors; (b) metal salt addition to N$_2$S$_2$O$_2$$^{2-}$ ligand appropriate for Fe^{2+}, Co^{2+}, Ni^{2+}, Cu^{2+}, and Zn^{2+}; (c) metal exchange with **Zn-1'-Ac$_2$** applies to Co^{2+}, Ni^{2+}, and Cu^{2+}.

complexes produced by route (a). In addition, the copper product obtained by route (b) was identical to that from reaction (c), the Cu^{2+}/Zn^{2+} transmetallation, *i.e.*, the [**Cu-1′-Ac₂**]₂ product.

Zinc/metal transmetallation

In a previous study, nickel was shown to rapidly replace zinc in the hexadentate $N_2S_2O_2$ ligand as shown in Fig. 3.[31] Similarly, on addition of a light pink solution of $Co(NO_3)_2$ to a colorless methanolic solution of **Zn-1′-Ac₂** an immediate color change to a deep magenta was observed, producing **Co-1′-Ac₂** that was isolated in >70% yield. Likewise, $Cu(NO_3)_2$ mixed with **Zn-1′-Ac₂** gave a 30% isolated yield of [**Cu-1′-Ac₂**]₂ (deep blue). The characteristic properties of **Co-1′-Ac₂** and [**Cu-1′-Ac₂**]₂ matched those of the direct synthesis, route (b), Fig. 4, products. Thus, a facile transmetallation reaction between the kinetically labile zinc center in **Zn-1′-Ac₂** and an exogenous metal ion occurs only with the aid of the acetate arms. It is notable that no exchange was observed between Zn^{2+} in **Zn-1′-Ac₂** and $Fe(NO_3)_2$.

Control experiments and qualitative rankings of transmetallations

Previous results[31] along with several control reactions provided insight into the metal exchange process. The addition of $Ni(NO_3)_2$ in the presence and absence of NaOAc to a stirred solution of [**Co-1′**]₂, both at 22 °C and 70 °C, resulted in the formation of metallo-aggregates rather than a quantitative exchange of metals, processes 1 and 2 of Fig. 5. However, if $Ni(NO_3)_2$ and $Na^+[ICH_2CO_2]^-$ are simultaneously added to a solution of [**Co-1′**]₂, process 3, Fig. 5, pure **Ni-1′-Ac₂** could be isolated from the reaction in a *ca.* 60% yield illustrating that the modification of the thiolate sulfurs through acetylation is needed for clean metal exchange between the $N_2S_2O_2$ ligand frameworks.

The results expressed in Fig. 4, route (c), give evidence for the ranking of metal exchange with Zn^{2+} in the $N_2S_2O_2$ ligand, *i.e.*, Co^{2+}, Ni^{2+}, and Cu^{2+} ions displace Zn^{2+}; the Fe^{2+} from $Fe(NO_3)_2$

however does not. Stepwise exchanges in a single flask readily monitored by color changes and UV-vis spectroscopy, beginning with **Fe-1′-Ac₂** find that Co^{2+} replaces Fe^{2+}; Ni^{2+} replaces Co^{2+}; and Cu^{2+} replaces Ni^{2+}. These qualitative results are consistent with the well-known Irving–Williams series.[37] More quantitative studies for Co^{2+} and Ni^{2+}, processes 4 and 5 in Fig. 5, yielded an approximate K_{eq} from isolated products, analyzed by UV-vis and mass spectroscopy. Both methods indicate the formation of about 20% **Co-1′-Ac₂** and 80% unreacted **Ni-1′-Ac₂**. From this data, equilibrium constants in MeOH solutions were estimated for the forward (Ni^{2+} replacement of Co^{2+}) and reverse (Co^{2+} replacement of Ni^{2+}) reactions to be *ca.* 2×10^3 and 5×10^{-4}, respectively. The equilibrium constants reported below were determined in experiments carried out in aqueous media.

The possibility of exchange or metal scrambling between N_2S_2 and $N_2S_2O_2$ binding sites was also explored. In the first case a mixture of **Ni-1′** and **Zn-1′-Ac₂** were dissolved in a methanol solution and stirred for 7 days over which time there was, from MS and UV-vis analysis, no indication of any reaction occurring. We conclude that nickel cannot be transferred from its tight N_2S_2 binding site; nor can the acetyl group be transferred from the zinc to the nickel thiolate sulfur. Likewise, the opposite conditions of a mixture of **Ni-1′-Ac₂** and [**Zn-1′**]₂, indicated no metal exchange occurred between the two complexes even after 7 days.

Properties of M-1′-Ac₂ complexes

Infrared data for the **M-1′-Ac₂** complexes in CH_2Cl_2 solutions are found in the Experimental section. All exhibit a strong solution IR stretch at *ca.* 1630 cm^{-1} corresponding to the acetate C=O group, with no apparent trend in the relative positions. Assignments of two prominent bands in the 1300's region for all are equivocal, but presumed to correspond to M–O or C–O stretches.

As described in the Experimental section, Gouy balance and Evans' method magnetic studies established that the octahedral complexes of Cu^{2+}, Ni^{2+}, Co^{2+}, and high-spin Fe^{2+} are paramagnetic with experimental magnetic moments largely matching the expected $\mu_{s.o.}$ values; the d^{10} Zn^{2+} derivative is diamagnetic.

The cyclic voltammograms for **Ni-1′-Ac₂** and **Co-1′-Ac₂** are shown in Fig. S1 and S3,† respectively. Both complexes show an oxidation event assigned to the reversible Ni^{2+}/Ni^{3+} couple at 0.69 V and a quasi-reversible Co^{2+}/Co^{3+} couple at −0.24 V. An irreversible event is seen at −2.33 V and −2.31 V for **Ni-1′-Ac₂** and **Co-1′-Ac₂**, respectively. Data relating to reversibility are as follows: for the **Ni-1′-Ac₂**, E_{pa}, E_{pc}, ΔE, and i_{pc}/i_{pa} are 0.656 V, 0.716 V, 60 mV, and 0.86, respectively; and for **Co-1′-Ac₂**, −0.390 V, −0.090 V, 300 mV, and 0.74, respectively.

X-ray diffraction analyses of molecular structures

Crystals of the **Co-1′-Ac₂**, **Fe-1′-Ac₂**, and [**Cu-1′-Ac₂**]₂ complexes were obtained as racemic mixtures from layering methanol solutions with diethyl ether. The structures were refined in the $P\bar{1}$ (triclinic), $P\bar{1}$ (triclinic), and $C2/c$ (monoclinic) space groups, respectively. The former two co-crystallize with two MeOH
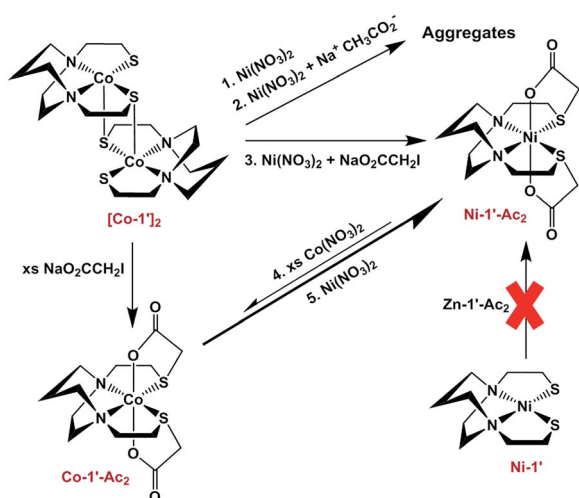

Fig. 5 Scheme illustrating various control reactions carried out during the investigation of metal exchange reactions.

molecules that are H-bonded to the free carboxylate oxygens, *vide infra*.

Fig. 6 shows the thermal ellipsoid renderings for the **Fe-1'-Ac$_2$** and **Co-1'-Ac$_2$** structures. The distorted octahedral **Co-1'-Ac$_2$** molecule contains a near perfect N_2S_2 plane with a mean atom deviation of 0.007 Å (without Co). The cobalt center is displaced from the best N_2S_2 plane by 0.001 Å. The Fe analog contains an average deviation of 0.011 Å from the N_2S_2 plane and the Fe displacement is 0.014 Å. Note that the O–M–O angles are ≠ 180° and are bent toward the M–S side of the molecule as observed in the previously reported Zn and Ni analogs.

The **[Cu-1'-Ac$_2$]$_2$** complex exists as a dimer resulting from detachment of one of the thioether arms which allows the carboxylate oxygens to bridge to a second copper center, Fig. 7. The copper centers thus display pentacoordination in a distorted square pyramidal structure, CuN_2SO_2, with τ value[38] of 0.015 and an almost ideal N_2OS plane (with a mean atom deviation of 0.051 Å). The Cu[II] metal is displaced from this N_2OS best plane by 0.208 Å and the Cu–Cu distance is 7.189 Å. Also of note, the two N_2OS planes present in the **[Cu-1'-Ac$_2$]$_2$** dimer intersect at an angle of 64.56°.

Table 1 lists crystallographic data and selected metric parameters for the three new complexes of this study along with **Ni-1'-Ac$_2$** and **Zn-1'-Ac$_2$**.[31] Note that the **Zn-1'-Ac$_2$** is completely analogous to the Co and Fe analogues. The M–S distances from Fe to Cu are found to diminish and then increase at the end with the **Zn-1'-Ac$_2$** complex, a trend which tracks their ionic radii and as noted by the Irving–Williams series.[37] The same trend can be seen with the M–N distances; however, the M–O bond distances actually increase across the row as the radii decrease. This is likely a result of the more drastic decrease in M–S distances coupled into the torsion angles through the acetate arm. Thus, the oxygen donors are prohibited from moving toward the metal center, but rather shift away as the metal ion gets smaller. Overall, the bond distances for the **Zn-1'-Ac$_2$** complex fall between those of the **Fe-1'-Ac$_2$** and **Co-1'-Ac$_2$** complexes.

For comparison with the analogous NiN_2S_2 that is *S*-modified by acetamide, AA, the structure of **[Ni-1'-AA$_2$]I$_2$** is shown in Fig. 8, along with **Ni-1'-Ac$_2$**. The metric parameters of **[Ni-1'-AA$_2$]**
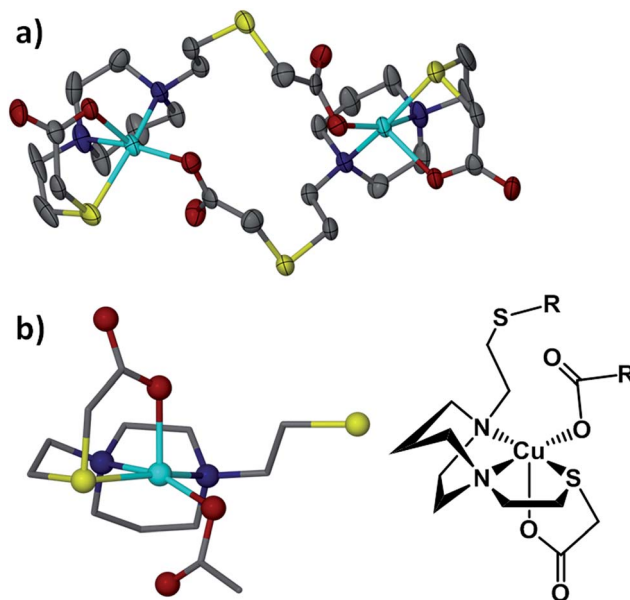
Fig. 7 Thermal ellipsoid plot of **[Cu-1'-Ac$_2$]$_2$** molecular structure showing (a) the carboxylate bridged dimer and (b) one unit of the dimer in ball and stick from XRD and in Chemdraw graphic, inverted and rotated by 90°.

I$_2$ largely track with the **Ni-1'-Ac$_2$** structure in terms of the first coordination sphere angles and bond distances. All compounds in the **M-1'-Ac$_2$** and **Ni-1'-AA$_2$** series co-crystallize with MeOH or H_2O in a H-bonded network that links the solvent molecules and the =O or –NH$_2$ groups that are directed into the interstitial space between molecules. Fig. S4† shows an example of this H-bonding network in **Co-1'-Ac$_2$**.

Equilibrium constants

Equilibrium constants of the metal exchange reactions were measured in aqueous solutions using UV-vis spectroscopy. Metal salts, see Table 2, and **M-1'-Ac$_2$** complexes, dissolved in
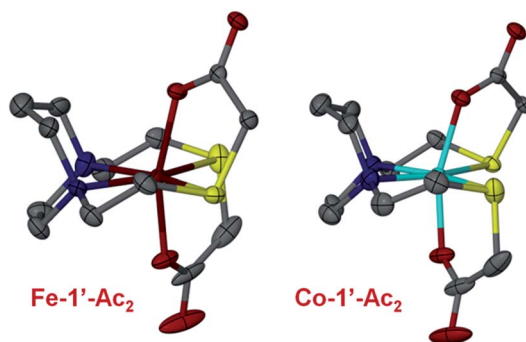
Fig. 6 Thermal ellipsoid plots shown at 50% for the **Fe-1'-Ac$_2$** and **Co-1'-Ac$_2$** molecular structures. Color code: N, blue; O, red; S, yellow; C, gray; Fe, dark red; Co, teal.

Table 1 Selected crystallographic data, bond distances, and angles of **Fe-1'-Ac$_2$**, **Co-1'-Ac$_2$**, **Ni-1'-Ac$_2$**,[27] **[Cu-1'-Ac$_2$]$_2$**, and **Zn-1'-Ac$_2$**[27]

	Fe-1'-Ac$_2$	Co-1'-Ac$_2$	Ni-1'-Ac$_2$	[Cu-1'-Ac$_2$]$_2$	Zn-1'-Ac$_2$
System	Triclinic	Triclinic	Monoclinic	Monoclinic	Triclinic
Space group	$P\bar{1}$	$P\bar{1}$	$P2_1$	$C2/c$	$P\bar{1}$
Solvation	2 MeOH	2 MeOH	3H$_2$O	1 MeOH	2 MeOH
Z	2	2	4	4	2
R-factor	5.76%	3.79%	5.72%	4.18%	3.68%
M–S$_{avg}$	2.532(2)	2.483(1)	2.399(3)	2.383(2)	2.577(1)
M–N$_{avg}$	2.178(4)	2.137(3)	2.094(7)	2.025(4)	2.165(3)
M–O$_{avg}$	2.029(3)	2.028(5)	2.056(6)	1.954(3)	2.042(3)
∠S–M–S	116.37(4)	113.10(7)	106.02(8)	92.60(1)^a	114.80(3)
∠N–M–N	74.6(1)	75.55(9)	77.8(3)	80.0(2)	75.6(1)
∠O–M–O	162.2(1)	160.7(2)	169.2(2)	102.5(1)^b	159.1(1)

^{a} ∠S–M–O from the N_2SO plane in the **[Cu-1'-Ac$_2$]$_2$** complex. ^{b} The oxygen atoms are *cis* in the **[Cu-1'-Ac$_2$]$_2$** structure rather than trans as observed in the other **M-1'-Ac$_2$** structures.
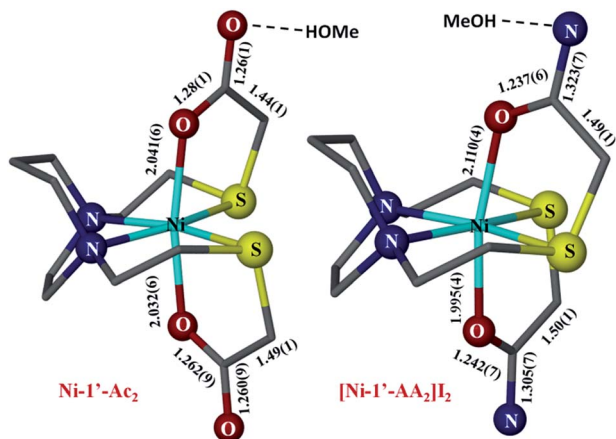
Fig. 8 Comparison of the metric parameters in **Ni-1′-Ac₂** (left) and [**Ni-1′-AA₂**]**I₂** (right). Hydrogen atoms, counter ions, and solvent molecules have been removed for clarity. Color coding as in Fig. 6; Ni in light blue.

water, were combined in a 1 : 1 ratio at 0.007–0.008 M concentrations and allowed to equilibrate for 3 h at 22 °C. The UV-vis spectra were then recorded and, in combination with molar absorptivity values at selected wavelengths, Table S1,† the concentrations of the species in solution at equilibrium were calculated.

$$\textbf{M-1′-Ac}_2 + \text{M′}(\text{H}_2\text{O})_x^{2+} \rightleftharpoons \textbf{M′-1′-Ac}_2 + \text{M}(\text{H}_2\text{O})_x^{2+} \quad (1)$$

$$K_{eq} = \frac{[\text{M′1′Ac}_2][\text{M}^{2+}]}{[\text{M1′Ac}_2][\text{M′}^{2+}]} \quad (2)$$

Thus, the equilibrium constants shown in Table 2 assumed that each metal is contained in one of the two forms present in eqn (1) and (2), see Chart S1† for equations used. Of the possible aggregates or mixed metal complexes in the likely complicated mechanism, *vide infra*, none are observed in the UV-vis monitor. In the following discussion, the exchange pairs are expressed as **M-1′-Ac₂**/M′²⁺ → **M′-1′-Ac₂**/M²⁺ and shortened to M/M′ and M′/M, respectively.

The values reported in Table 2 are averages of triplicate experiments calculated at a single wavelength as indicated. The thus obtained equilibrium constants measured according to establishment of equilibrium from two directions, *i.e.*, for the Zn/Co and Co/Zn exchange pairs, are, as expected, the mathematical inverse of each other. Likewise those for the Zn/Ni and

Ni/Zn exchange pairs are, within the error of measurement, consistent. However the Co/Ni (K_{eq} = 210) and Ni/Co (K_{eq} = 0.0002) exchange pairs show discrepancies in the values that we suggest are within error of molar absorptivity measurements. The presence of four UV-vis active species in solution further complicates accurate measurements of the equilibrium constants using the available simple techniques.

Overall, the estimated K_{eq} values serve to accentuate the exchange hierarchy, which is again consistent with the Irving–Williams series $\text{Zn}^{2+} < \text{Co}^{2+} < \text{Ni}^{2+}$.[37]

Kinetic studies

Monitors of the addition of $\text{Ni}(\text{NO}_3)_2$, $\text{Co}(\text{NO}_3)_2$, or $\text{Cu}(\text{NO}_3)_2$ to a MeOH solution of **Zn-1′-Ac₂** found reactions completed within the time of mixing and thus too fast for rate measurements by our available techniques, Fig. S5.† Thus, the displacement of **Co-1′-Ac₂** by Ni^{2+} in MeOH was selected as a reaction sufficiently slow for kinetic monitoring. Fig. 9 and S6† display full UV-vis scans for this metal exchange reaction, with alternate pseudo first order conditions for each reactant. Fig. 9 includes an inset showing the UV-vis spectra of pure **Co-1′-Ac₂** and **Ni-1′-Ac₂**. The ten-fold excess of **Co-1′-Ac₂** reacting with Ni^{2+} in MeOH show the UV-vis absorptions at 362 and 845 nm to increase while a peak at 487 nm decreases in absorbance, Fig. 9. If the opposite
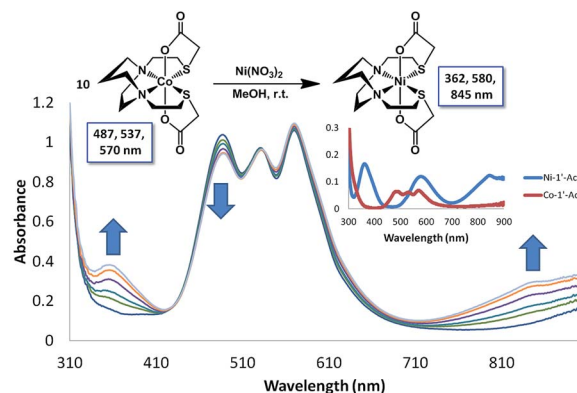

Fig. 9 UV-vis traces in MeOH for the reaction of Ni^{2+} with a ten-fold excess of **Co-1′-Ac₂**. An inset shows the UV-vis spectra for the pure **Ni-1′-Ac₂** and **Co-1′-Ac₂**. The peaks at 362 and 845 nm increase as a result of **Ni-1′-Ac₂** formation and a decrease at 487 nm as **Co-1′-Ac₂** undergoes transmetallation. Reaction was monitored until no further change in the UV-vis spectrum was observed, requiring approximately 20 min at room temperature.

Table 2 Equilibrium constants measured in water by UV-vis spectroscopy at 0.007–0.008 M concentrations and 22 °C for metal exchange reactions. In parenthesis is the wavelength used to calculate each value

	Zn(BF₄)₂	CoSO₄	NiSO₄
Zn-1′-Ac₂	—	4.80 ± 0.18 (527 nm)	210 ± 40 (359 nm)
Co-1′-Ac₂	0.20 ± 0.01 (527 nm)	—	230 ± 100 (575 nm)
Ni-1′-Ac₂	0.01 ± 0.001 (359 nm)	0.0004 ± 0.0004 (575 nm)	—

molar ratio is used (1 **Co-1'-Ac₂**: 10 Ni²⁺) then the peaks at 362, 580, and 845 nm increase corresponding to the formation of **Ni-1'-Ac₂**; the peak at 487 nm decreases as **Co-1'-Ac₂** undergoes metal exchange, Fig. S6.†

In a typical kinetics experiment the **Co-1'-Ac₂** concentration was 0.0050 M and the Ni(NO₃)₂ was in 12.5, 25, or 50-fold excess. The reactions were monitored at ambient temperature by appearance of the UV-vis band at 845 nm, with data collection started as soon as the two solutions were injected into the cuvette, and followed to completion. The linearity of the natural log plot of the absorbance at 845 nm, *versus* time, Fig. 10, indicates that the reaction is first order in the **Co-1'-Ac₂** complex.

The order of reaction dependence on Ni²⁺ was determined by monitoring the exchange at multiple concentrations of excess Ni²⁺. A plot of k_{obs} *vs.* [Ni²⁺], Fig. S7,† is linear with a *y*-intercept of nearly zero indicating a first-order dependence for Ni²⁺. Thus, the complete bimolecular rate law is shown below with a first order dependence of both **Co-1'-Ac₂** and Ni²⁺.

$$\text{rate} = k_{obs}[\textbf{Co-1'Ac}_2]^1 \quad (3)$$

$$k_{obs} = k[\text{Ni}^{2+}]^n \quad (4)$$

$$\text{rate} = k[\textbf{Co-1'Ac}_2]^1[\text{Ni}^{2+}]^1 \quad (5)$$

The temperature dependence of the rate constant, k, was measured over a 37 K range (286–313 K), Fig. S8,† for the conversion of **Co-1'-Ac₂** to **Ni-1'-Ac₂**. During these experiments the **Co-1'-Ac₂** solution was equilibrated in the temperature-controlled cuvette holder before injection of the temperature-adjusted Ni(NO₃)₂ solution. The temperatures, k_{obs}, and k values are listed in Table 3.

Activation parameters for the formation of **Ni-1'-Ac₂** from **Co-1'-Ac₂**; were determined by an Eyring analysis which found $\Delta H^{\ddagger}$ of 15.7 ± 0.7 kcal mol⁻¹ and a $\Delta S^{\ddagger}$ of −14.3 ± 2.3 e.u., Fig. 11. The $\Delta G^{\ddagger}$ can be calculated at 298 K as 19.9 ± 0.7. The small $\Delta H^{\ddagger}$ and negative $\Delta S^{\ddagger}$ values are indicative of an associative mechanism for the Co/Ni transmetallation reaction, consistent with

Table 3 Kinetic parameters obtained from the natural log plots from varying temperature for the reaction of **Co-1'-Ac₂** with excess Ni(NO₃)₂ in MeOH. The concentration of **Co-1'-Ac₂** was 4.75×10^{-3} M and Ni(NO₃)₂ was 0.119 M *i.e.*, 1 : 25 ratio

T (K)	k_{obs} (s⁻¹)	k (M⁻¹ s⁻¹)
286	7.32×10^{-3}	4.65×10^{-3}
293	3.93×10^{-3}	9.04×10^{-3}
303	2.54×10^{-3}	2.14×10^{-2}
308	1.07×10^{-3}	3.31×10^{-2}
313	5.51×10^{-4}	6.17×10^{-2}
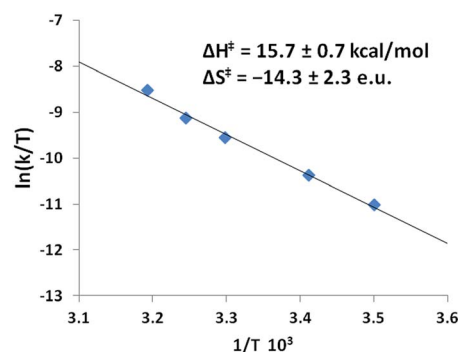
Fig. 11 Eyring plot obtained from the dependence of k on temperature for **Co-1'-Ac₂** + 25× Ni(NO₃)₂ in MeOH. The equation for the best-fit line is $y = -7.8938x + 16.557$ with an R^2 value of 0.993. The analogous Arrhenius plot can be found in Fig. S10.†

the bimolecular rate law above. $\Delta H^{\ddagger}$ and $\Delta S^{\ddagger}$ may represent composite values of both activation parameters and equilibrium constants dependent on the rate limiting step in the mechanism (*vide infra*).

Experimental section

General methods and materials

Solvents were dried and degassed using a Bruker solvent system. The products are air stable; however, as a precautionary measure, all reactions were carried out under an inert atmosphere of argon using standard Schlenk procedures unless otherwise noted. The acetylated products can be extremely hygroscopic, necessitating exclusion of moisture. Separations used silica gel chromatography both for thin layer and column purifications. Reagents were used as acquired from standard vendors. The bis(2-mercaptoethyl)-1,4-diazacycloheptane (H₂bme-dach),[12] *N,N'*-bis(2-mercaptoethyl)-1,4-diazacycloheptane zinc(II) dimer [**Zn-1'**]₂,[39] *N,N'*-bis(2-mercaptoethyl)-1,4-diazacycloheptane iron(II) dimer [**Fe-1'**]₂,[40] *N,N'*-bis(2-mercaptoethyl)-1,4-diazacycloheptane cobalt(II) dimer [**Co-1'**]₂,[40] *N,N'*-bis(2-mercaptoethyl)-1,4-diazacycloheptane nickel(II) **Ni-1'**,[12] 1,4-diazacycloheptane-1,4-diylbis(3-thiapentanoato) zinc(II) **Zn-1'-Ac₂**,[31] and 1,4-diazacycloheptane-1,4-diylbis(3-thiapentanoato)nickel(II) **Ni-1'-Ac₂**,[31] were synthesized according to published procedures. Additional details for the synthesis of **Co-1'-Ac₂**, **Fe-1'-Ac₂** and [**Cu-1'-Ac₂**]₂ are available in the ESI.†
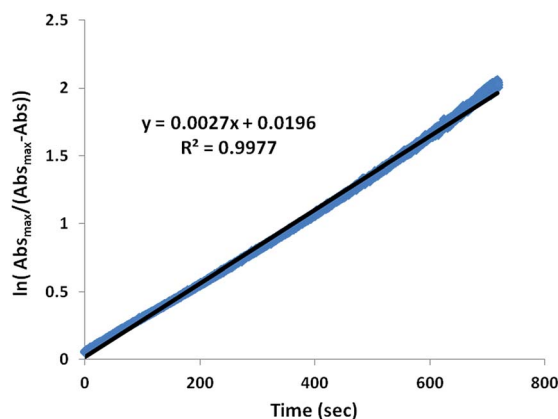

Fig. 10 Sample plot of the natural log of the change of absorbance at 845 nm (appearance of **Ni-1'-Ac₂**) *versus* time for the reaction of a 25-fold excess of Ni(NO₃)₂ with **Co-1'-Ac₂** at room temperature. A linear fit (black line) of the data (blue points) yields a k_{obs} of 2.65×10^{-3} s⁻¹.

Physical measurements

Elemental analyses were performed by Atlantic Microlab, Inc. Norcross, GA, USA. Electrospray ionization mass spectrometry (ESI-MS) was performed by the Laboratory for Biological Mass Spectrometry at Texas A&M University. Solution infrared spectra were recorded on a Bruker Tensor 37 Fourier Transform-IR spectrometer, using a CaF_2 cell with 0.2 mm path length. UV-visible spectra were obtained using a Shimadzu UV-2450 spectrophotometer with 1.0 cm path length quartz cells. Cyclic voltammograms were recorded on a BAS-100A electrochemical analyzer. All experiments were performed at room temperature under Ar in MeCN solution containing 0.1 M $[n\text{-}Bu_4N][PF_6]$ as the electrolyte, with a 3.0 mm glassy carbon working electrode, an $Ag/AgNO_3$ reference electrode, and a Pt coil counter electrode. All values have been internally referenced to the Fc/Fc^+ couple.

X-ray crystallography

The X-ray data for **Ni-1′-AA₂**, **Co-1′-Ac₂**, **Fe-1′-Ac₂**, and **[Cu-1′-Ac₂]₂** (CCDC #1407471–1407474) were obtained on a single-crystal APEX2 CCD diffractometer (Mo Kα radiation, $\lambda = 0.71073$ Å) in the X-ray Diffraction Laboratory at Texas A&M University. Crystal samples were coated in mineral oil, affixed to a Nylon loop, and placed under streaming N_2 (110/150 K). The structures were solved by direct methods. H atoms were placed at idealized positions and refined with fixed isotropic displacement parameters, and anisotropic displacement parameters were employed for all non-hydrogen atoms. The following programs were used: data collection and reduction, APEX2;[41] absorption correction SADABS;[42] cell refinement SHELXTL;[43] structure solutions, SHELXS-97;[43] and structure refinement, SHELXL-97.[43] The final data presentation and structure plots were generated in X-Seed Version 2.0.[44] CIF files were prepared for publication using WinGX and its included programs.[45] Data acquisition and refinement data are in ESI.†

Synthesis and characterization

1,4-Diazacycloheptane-1,4-diylbis(3-thiapentanamide) nickel(ɪɪ) iodide, [Ni-1′-AA₂][I]₂

NiN₂S₂ templated synthesis. A portion of **Ni-1′** (0.25 g, 0.90 mmol) was placed in a 100 mL Schlenk flask and degassed prior to addition of 30 mL MeCN. Iodoacetamide, AA, (0.35 g, 1.90 mmol) in 20 mL MeCN was cannulated into the stirring **Ni-1′** solution. The reaction mixture was stirred at 22 °C for 48 h yielding a blue precipitate. The mixture was filtered anaerobically and the solid was washed with 3 × 5 mL MeCN and 3 × 10 mL Et_2O and dried *in vacuo* to yield 0.48 g (0.74 mmol, 82%) of **[Ni-1′-AA₂][I]₂** solid. ESI-mass spectrum in CH_3OH: $[NiN_4S_2O_2\text{-}C_{13}H_{26}]^{2+}$ $m/z = 196.0$ (100%) $[NiN_4S_2O_2C_{13}H_{26} + H^+]^+$ $m/z = 391.0$ (44%). UV-vis (CH_3OH): λ_{max}, nm (ε, M^{-1} cm^{-1}) = 831 (37), 573 (38), 358 (56), 255 (6580) nm. IR (in MeOH, cm^{-1}): 1673 (*vs.*, sharp). Magnetic moment, Guoy Balance: 2.93 B.M. Elem. anal. calc'd for **[Ni-1′-AA₂][I]₂**•2MeOH, $NiN_4S_2O_4C_{15}H_{34}I_2$ (found): C: 25.34 (25.24), H: 4.82 (4.72), N: 7.88 (7.62).

Templated synthesis, route (a)

1,4-Diazacycloheptane-1,4-diylbis(3-thiapentanoic) cobalt(ɪɪ), **Co-1′-Ac₂**. A sample of **[Co-1′]₂** (0.50 g, 0.90 mmol) within a 250 mL Schlenk flask was dissolved in 50 mL of dry MeOH, producing a green solution. Sodium iodoacetate, Na^+IAc^-, (0.84 g, 4.0 mmol) in 40 mL MeOH, was added *via* cannula to the stirring **[Co-1′]₂** solution. The solution became a dark red/brown and stirring was continued for 24 h; the solvent was reduced *in vacuo* and the mixture was filtered to remove any NaI formed. The filtrate was chromatographed on a silica gel column (3 × 20 cm) using a 1 : 1 MeOH : MeCN solvent mixture as eluent. An initial band of yellow material was discarded and the magenta product, with an R_f value of 0.45, was collected. The solvent was removed *in vacuo*, and precipitation of a powder forced with addition of ether. The product was collected by filtration, washed 3× with ether, and dried *in vacuo* yielding 0.40 g (0.88 mmol, 98%) of **Co-1′-Ac₂**·2MeOH solid. ESI-mass spectrum in CH_3OH: $[CoN_2S_2O_4\text{-}C_{13}H_{22} + Na^+]^+$ $m/z = 416$ (27%). UV-vis (CH_3OH): λ_{max}, nm (ε, M^{-1} cm^{-1}) = 570 (29), 537 (28), 487 (30), 279 (408) nm. IR (in CH_2Cl_2, cm^{-1}): 1627 (*vs.*, sharp), 1348 (m), 1329 (m). Cyclic voltammetry: $E_{1/2} = -240$ mV *vs.* Fc/Fc^+ in MeCN assigned to the Co^{III}/Co^{II} couple. Magnetic moment, Guoy balance: 4.79 B.M. Elem. anal. calc'd for **Co-1′-Ac₂**·2MeOH, $CoN_2S_2O_6C_{15}H_{30}$ (found): C: 39.38 (39.09), H: 6.61 (6.03), N: 6.12 (6.42).

1,4-Diazacycloheptane-1,4-diylbis(3-thiapentanoic) iron(ɪɪ), **Fe-1′-Ac₂**. As in the cases above, **Fe-1′-Ac₂** solid was isolated in 72% yield. ESI-mass spectrum in CH_3OH: $[FeN_2S_2O_4C_{13}H_{22} + H^+]^+$ $m/z = 391$. UV-vis (CH_3OH): λ_{max}, nm (ε, M^{-1} cm^{-1}) = 346 (2660), 280 (1560) nm. IR (in CH_2Cl_2, cm^{-1}): 1631 (*vs.*, sharp), 1348 (m), 1327 (m).

1,4-Diazacycloheptane-1,4-diylbis(3-thiapentanoic)copper(ɪɪ), **[Cu-1′-Ac₂]₂**. As a discrete Cu^{2+} complex analogous to **Ni-1′** or **[Co-1′]₂**, **Cu-1′** is not known, thus a templated synthesis was not attempted.

Hexadentate N₂S₂O₂ ligand synthesis followed by metallation, route (b)

Co-1′-Ac₂. The H_2bme-dach ligand (0.50 g, 2.3 mmol) was placed in a 500 mL Schlenk flask and dissolved in 50 mL MeOH. To this flask Na^+IAc^- (1.0 g, 5.0 mmol) in 50 mL MeOH was added. The pale yellow solution was magnetically stirred for 18 h before it was used *in situ*. To the stirring acetylated bme-dach ligand solution, $Co(NO_3)_2$ (0.66 g, 2.3 mmol) was added as a clear pink solution in 50 mL of dry MeOH whereupon a magenta color developed. The solution volume was partially reduced *in vacuo* before filtering to remove Na^+ salts formed during the reaction. Addition of Et_2O resulted in precipitation of a magenta solid, which was isolated by filtration. This powder was redissolved in MeOH and chromatographed through a silica gel column with MeOH as the eluent yielding 0.36 g (0.92 mmol, 40%). The properties of this product matched those from the templated synthesis, route (a).

Fe-1′-Ac₂. In a similar manner, **Fe-1′-Ac₂** solid was isolated in 66% yield from the reaction of $Fe(NO_3)_2$ and the $N_2S_2O_2$ ligand. The product had identical characteristics as the product from route (a).

[Cu-1′-Ac₂]₂. The reaction of $Cu(NO_3)_2$ and the $N_2S_2O_2$ ligand was performed similar to the cobalt case above to yield 24% **[Cu-**

$1'$-$Ac_2]_2$ solid. ESI-mass spectrum in CH_3OH: $[CuN_2S_2O_4C_{13}H_{22}$ + $H^+]^+$ m/z = 398. UV-vis (CH_3OH): λ_{max}, nm (ε, M^{-1} cm^{-1}) = 607 (202), 348 (2660), 287 (1560) nm. IR (in CH_2Cl_2, cm^{-1}): 1631 (vs., sharp), 1347 (m), 1329 (m). $E_{1/2}$ = −360 mV vs. Fc/Fc$^+$ in CH_2Cl_2 for the Cu^{II}/Cu^I couple. Magnetic moment, Evans method: 1.46 B.M. Elem. anal. calc'd for $[Cu$-$1'$-$Ac_2]_2 \cdot 2H_2O$, $CuN_2S_2O_5C_{13}H_{24}$ (found): C: 37.53 (37.04), H: 5.81 (5.76), N: 6.73 (6.64).

Metal exchange into Zn-$1'$-Ac_2, route (c)

Co-$1'$-Ac_2. To a 0.20 g, 0.51 mmol, sample of **Zn-$1'$-Ac_2**, 75 mL of MeOH was added, producing a clear colorless solution to which was added 0.15 g, 0.51 mmol of $Co(NO_3)_2$ as a light pink solution in 25 mL dry MeOH. The mixture was stirred for 24 h. The solid magenta product was isolated as above to yield 0.14 g (0.37 mmol, 72%); characterization matched above results.

Fe-1-Ac_2. Transmetallation between Fe^{2+} from $Fe(NO_3)_2$ and **Zn-$1'$-Ac_2** did not occur in MeOH.

$[Cu$-$1'$-$Ac_2]_2$. Analogous to the cobalt reaction $[Cu$-$1'$-$Ac_2]_2$ could be isolated in 30% yield as a blue solid. Characterization matched that obtained by route (b).

Control reactions: metal exchange between N_2S_2 bound and nitrate salts

$[Co$-$1']_2$ + $Ni(NO_3)_2$. The cobalt dimer $[Co$-$1']_2$ (0.050 g, 0.18 mmol) and $Ni(NO_3)_2$ (0.052 g, 0.18 mmol) were placed in a 30 mL vial followed by addition of 20 mL of MeOH. The solution was stirred overnight both at 22 °C (trial 1) and 70 °C (trial 2); no changes in UV-vis spectra were observed.

$[Co$-$1']_2$ + $Ni(NO_3)_2$ + $Na^+CH_3COO^-$. A 30 mL vial was charged with the cobalt dimer $[Co$-$1']_2$ (0.050 g, 0.18 mmol), $Ni(NO_3)_2$ (0.052 g, 0.18 mmol), and 20 equiv. of NaOAc (0.299 g, 0.36 mmol); these were dissolved in 35 mL of MeOH. The resulting mixture was stirred overnight at 22 °C. No change was observed in the UV-vis spectrum.

$[Co$-$1']_2$ + $Ni(NO_3)_2$ + $Na^+CH_3COO^-$ with heating. The above reaction conditions were repeated with the reaction stirring at 70 °C overnight. No changes were observed.

$[Co$-$1']_2$ + $Ni(NO_3)_2$ + $Na^+ICH_2COO^-$. The cobalt dimer $[Co$-$1']_2$ (0.050 g, 0.18 mmol), $Ni(NO_3)_2$ (0.052 g, 0.18 mmol), and 20 equiv. of $Na^+ICH_2COO^-$ (0.015 g, 0.072 mmol) were added to a 30 mL vial and dissolved in 20 mL of MeOH. The solution was stirred overnight at 22 °C. As no change was observed when compared to control reaction without $Na^+ICH_2COO^-$, an additional 8/5 equiv. of $Na^+ICH_2COO^-$ (0.060 g, 0.29 mmol) in 5 mL MeOH was added and stirred overnight. Again, no change was observed a further 18 equiv. of $Na^+ICH_2COO^-$ (0.68 g, 3.25 mmol) in 10 mL MeOH was added and the solution was stirred overnight. The reaction mixture was then purified by silica gel column chromatography. The blue band was collected and reduced in vacuo. Et_2O was added and the mixture left overnight at 22 °C to isolate 0.041 g (0.10 mmol, 58%) of **Ni-$1'$-Ac_2**.

$[Co$-$1']_2$ + $Ni(NO_3)_2$ + $Na^+ICH_2COO^-$ with heating. The above reaction conditions were repeated with the reactants stirred at 70 °C and product purified by the same means to yield 0.043 g (0.11 mmol, 59%) of **Ni-$1'$-Ac_2**.

Ni-$1'$-Ac_2 + $Co(NO_3)_2$. A 100 mL Schlenk flask was charged with **Ni-$1'$-Ac_2** (0.050 g, 0.13 mmol) and $Co(NO_3)_2$ (0.037 g, 0.13 mmol) and degassed prior to the addition of 25 mL MeOH. No exchange product was observed by UV-vis spectroscopy under these conditions so an additional 9 equiv. of $Co(NO_3)_2$ (0.33 g, 1.14 mmol) in 10 mL MeOH was added and stirred for 6 h. No product formation was observed by UV-vis analysis so a further 90 equiv. of $Co(NO_3)_2$ (3.33 g, 11.44 mmol) in 15 mL was added. The reaction volume was reduced in vacuo and the mixture components were separated by silica gel column chromatography using MeOH as an eluent. The $M(NO_3)_2$ salts elute first. A second blue/purple band, was collected and the volume was reduced in vacuo. UV-vis and mass spec analysis was used to quantify the amount of **Co-$1'$-Ac_2** (18–19%) formed since the **M-$1'$-Ac_2** species could not be separated from one another.

Ni-$1'$ + Zn-$1'$-Ac_2. A 100 mL Schlenk flask was charged with **Ni-$1'$** (0.050 g, 0.18 mmol) and **Zn-$1'$-Ac_2** (0.072 g, 0.18 mmol) and degassed. To this 50 mL of MeOH was added yielding a brown solution. After stirring overnight at room temperature no **Ni-$1'$-Ac_2** formation was observed by UV-vis spectroscopy. The solution was then stirred overnight at 70 °C and still no **Ni-$1'$-Ac_2** was observable by UV-vis spectroscopy.

Conclusions

The N_2S_2 ligand binding site has been found to be largely inert to metal exchange, rather yielding S-based aggregation products of various structural types when MN_2S_2 complexes are exposed to exogenous metals.[9,46] Such a tight binding characteristic of the tetradentate N_2S_2 ligands is lessened on S-alkylation. For example, S-methylation of $[Zn(bme$-$dach)]_2$ with MeI results in deligation of the newly formed thioethers and coordination of the
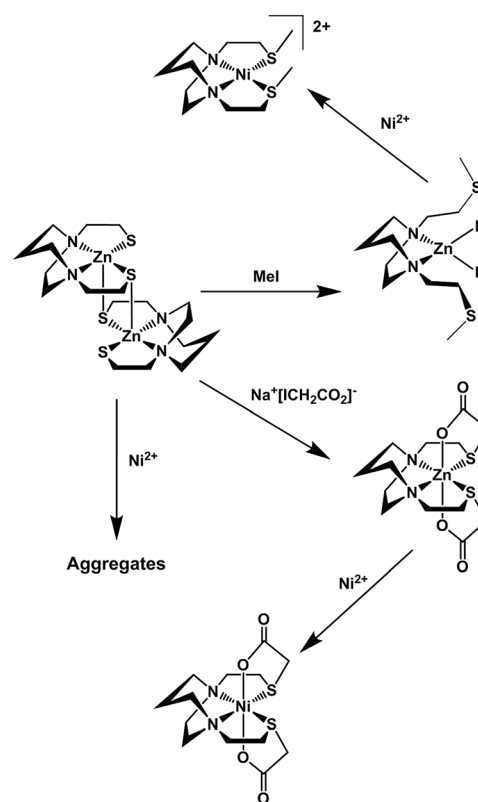

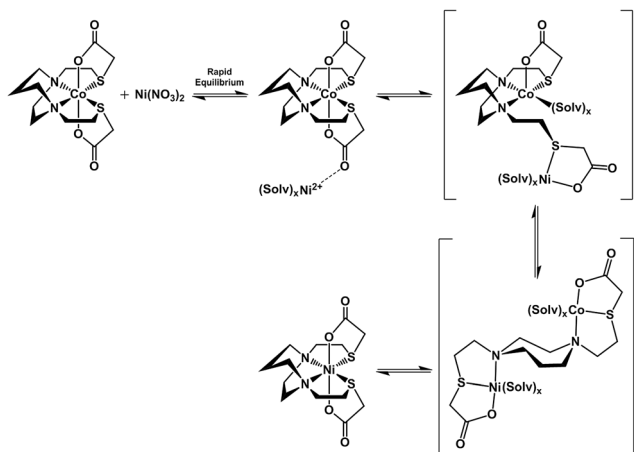**Fig. 12** Reactivity of $[Zn$-$1']_2$ toward alkylation or metallation.

Fig. 13 Proposed mechanism for the ligand unwrapping/wrapping process involved in metal exchange. Brackets indicate proposed intermediates.

Fig. 14 The X-ray crystal structure of (bme-dach)(CH$_2$OH)$_2$ which highlights the 7-membered diazacycle with the nitrogen lone pairs anti to each other and hydrogen bonding to the respective pendent −OH groups. The ligand was derived from the reaction of H$_2$bme-dach with paraformaldehyde in chloroform.

iodide ions yielding a tetrahedral ZnN$_2$I$_2$ as shown in Fig. 12.[13] The zinc is readily displaced by nickel, whereupon the thioether sulfur reclaims the metal binding in square planar coordination geometry. However, if the alkylation agent creates additional donor atoms within the ligand framework as in the iodoacetamide and iodoacetate derivatives, the chelate effect might be expected and indeed does keep the poor thioether donors bound to the Zn in a hexacoordinate, octahedral ZnN$_2$S$_2$O$_2$ site. However, such S-modification with sodium iodoacetate can also render the metal center labile and replaceable by exogenous metal ions through interaction with the available carboxylate oxygen atoms. The proposed mechanism resulting from this interaction entails a ligand unwrapping/rewrapping process, Fig. 13, leading to facile metal exchange rather than aggregation products. Modeled after the mechanistic suggestions of Margerum, *et al.*, the rate determining step is expected to involve the M–N bond-breaking/ forming step to give a bimetallic intermediate.[1,30]

Lending veracity to the proposed intermediates of Fig. 13, are two crystal structures: first, the [Cu-1'-Ac$_2$]$_2$ dimer, Fig. 7, finds carboxylate oxygens bound to copper resulting from one of the ligand arms which has become partially "unwrapped". The second is a structure of an N$_2$S$_2$O$_2$ free ligand based on bismercaptoethane-diazacycloheptane that has been S-alkylated by paraformaldehyde (CCDC #1407475). The diazacycle of the resulting molecule is in a conformation that would allow it to bridge to two metals using the inverted nitrogens. As shown, the Bronsted acid proton of the OH group replaces the Lewis acidic metals, Fig. 14.

Thus even with what would appear to be a very rigid ligand framework, and the requirement of bond breaking processes expected to have a high energy barrier, the unwrapping/ rewrapping process gains feasibility by the multiple interactions resulting from the additional carboxylate functionality. Of prime significance, this work illustrates a consequence of S-acetylation that to our knowledge has not been previously expressed, *i.e.*, a pathway for metal exchange. A wider application of such sequential binding/rebinding mechanisms
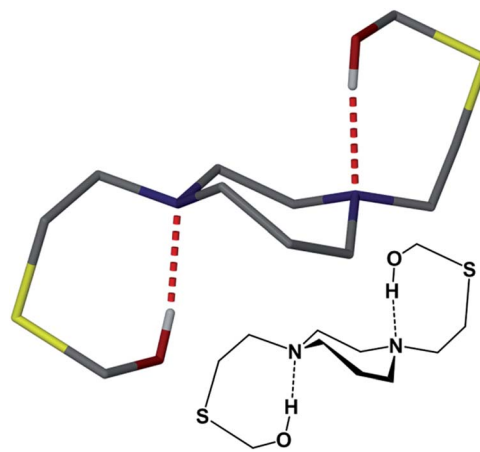
involving oxygen, nitrogen, and sulfur donors is likely in many metal transport processes. For example, the methanobactin Cu$^+$ chelator ultimately produces a four-coordinate N$_2$S$_2$ site for Cu$^+$,[47] with an uptake/release mechanism that involves peptide amido groups for which precise pathways are difficult to mimic.

Acknowledgements

Notes and references

1 D. W. Margerum, in *Mechanistic Aspects of Inorganic Reactions*, American Chemical Society, 1982, vol. 198, ch. 1, pp. 3–38.

2 G. J. Colpas and R. P. Hausinger, *J. Biol. Chem.*, 2000, **275**, 10731–10737.

3 J. Kuchar and R. P. Hausinger, *Chem. Rev.*, 2004, **104**, 509–526.

4 Y. Li and D. B. Zamble, *Chem. Rev.*, 2009, **109**, 4617–4643.

5 T. I. Doukov, L. C. Blasiak, J. Seravalli, S. W. Ragsdale and C. L. Drennan, *Biochemistry*, 2008, **47**, 3474–3483.

6 T. Arakawa, Y. Kawano, S. Kataoka, Y. Katayama, N. Kamiya, M. Yohda and M. Odaka, *J. Mol. Biol.*, 2007, **366**, 1497–1509.

7 S. Nagashima, M. Nakasako, N. Dohmae, M. Tsujimura, K. Takio, M. Odaka, M. Yohda, N. Kamiya and I. Endo, *Nat. Struct. Mol. Biol.*, 1998, **5**, 347–351.

8 L. Song, M. Wang, J. Shi, Z. Xue, M.-X. Wang and S. Qian, *Biochem. Biophys. Res. Commun.*, 2007, **362**, 319–324.

9 J. A. Denny and M. Y. Darensbourg, *Chem. Rev.*, 2015, **115**, 5248–5273.

10 P. J. Farmer, T. Solouki, D. K. Mills, T. Soma, D. H. Russell, J. H. Reibenspies and M. Y. Darensbourg, *J. Am. Chem. Soc.*, 1992, **114**, 4601–4605.

11 D. K. Mills, J. H. Reibenspies and M. Y. Darensbourg, *Inorg. Chem.*, 1990, **29**, 4364–4366.

12 J. J. Smee, M. L. Miller, C. A. Grapperhaus, J. H. Reibenspies and M. Y. Darensbourg, *Inorg. Chem.*, 2001, **40**, 3601–3605.

13 C. A. Grapperhaus, T. Tuntulani, J. H. Reibenspies and M. Y. Darensbourg, *Inorg. Chem.*, 1998, **37**, 4052–4058.

14 J. D. Hempel and R. Pietruszko, *J. Biol. Chem.*, 1981, **256**, 10889–10896.

15 C. H. Reynolds and J. S. McKinley-McKee, *Eur. J. Biochem.*, 1969, **10**, 474–478.

16 K. H. Dahl and J. S. McKinley-McKee, *Eur. J. Biochem.*, 1981, **118**, 507–513.

17 O. Boutureira and G. J. L. Bernardes, *Chem. Rev.*, 2015, **115**, 2174–2195.

18 N. A. Zorin, B. Dimon, J. Gagnon, J. Gaillard, P. Carrier and P. M. Vignais, *Eur. J. Biochem.*, 1996, **241**, 675–681.

19 J. J. Smee, D. C. Goodman, J. H. Reibenspies and M. Y. Darensbourg, *Eur. J. Inorg. Chem.*, 1999, 539–546.

20 R. L. Lundblad, in *Chemical Reagents for Protein Modification*, CRC Press, 4th edn, 2014, ch. 7, pp. 217–338.

21 R. D. Hancock and A. E. Martell, *Chem. Rev.*, 1989, **89**, 1875–1914.

22 A. I. Anzellotti, Q. Liu, M. J. Bloemink, J. N. Scarsdale and N. Farrell, *Chem. Biol.*, 2006, **13**, 539–548.

23 J. Emsley, ed. *Nature's Building Blocks: An A-Z Guide to the Elements*, Oxford University Press, Oxford, U.K, 2003.

24 D. S. Auld, *BioMetals*, 2009, **22**, 141–148.

25 I. Bertini, H. B. Gray, S. J. Lippard and J. Valentine, in *Bioinorganic Chemistry*, University Science Books, Mill Valley, CA, 1994, ch. 2, pp. 37–106.

26 J. M. Berg and H. A. Godwin, *Annu. Rev. Biophys. Biomol. Struct.*, 1997, **26**, 357–371.

27 R. Gasper, A. Scrima and A. Wittinghofer, *J. Biol. Chem.*, 2006, **281**, 27492–27502.

28 M. R. Leach, S. Sandal, H. Sun and D. B. Zamble, *Biochemistry*, 2005, **44**, 12229–12238.

29 E. C. Escudero-Adán, J. Benet-Buchholz and A. W. Kleij, *Inorg. Chem.*, 2007, **46**, 7265–7267.

30 T. J. Bydalek and D. W. Margerum, *J. Am. Chem. Soc.*, 1961, **83**, 4326–4329.

31 E. Almaraz, J. A. Denny, W. S. Foley, J. H. Reibenspies, N. Bhuvanesh and M. Y. Darensbourg, *Dalton Trans.*, 2009, 9496–9502.

32 D. C. Goodman, T. Tuntulani, P. J. Farmer, M. Y. Darensbourg and J. H. Reibenspies, *Angew. Chem., Int. Ed.*, 1993, **32**, 116–119.

33 R. K. Steinhaus and R. L. Swann, *Inorg. Chem.*, 1973, **12**, 1855–1860.

34 L. Kolopajlo, *J. Coord. Chem.*, 2006, **59**, 891–899.

35 Y. Li, A. E. Martell, R. D. Hancock, J. H. Reibenspies, C. J. Anderson and M. J. Welch, *Inorg. Chem.*, 1996, **35**, 404–414.

36 J. A. Denny, W. S. Foley, E. Almaraz, J. H. Reibenspies, N. Bhuvanesh and M. Y. Darensbourg, *Dalton Trans.*, 2012, **41**, 143–148.

37 H. Irving and R. J. P. Williams, *J. Chem. Soc.*, 1953, 3192–3210.

38 A. W. Addison, T. N. Rao, J. Reedijk, J. van Rijn and G. C. Verschoor, *J. Chem. Soc., Dalton Trans.*, 1984, 1349–1356.

39 E. Almaraz, Q. A. de Paula, Q. Liu, J. H. Reibenspies, M. Y. Darensbourg and N. P. Farrell, *J. Am. Chem. Soc.*, 2008, **130**, 6272–6280.

40 C.-Y. Chiang, J. Lee, C. Dalrymple, M. C. Sarahan, J. H. Reibenspies and M. Y. Darensbourg, *Inorg. Chem.*, 2005, **44**, 9007–9016.

41 Bruker, in *APEX2*, Bruker AXS Inc., Madison, Wisconsin, USA, 2007.

42 Bruker, in *SADABS*, Bruker AXS Inc., Madison, Wisconsin, USA, 2001.

43 G. Sheldrick, *Acta Crystallogr., Sect. A: Cryst. Phys., Diffr., Theor. Gen. Crystallogr.*, 2008, **64**, 112–122.

44 L. J. Barbour, *J. Supramol. Chem.*, 2001, **1**, 189–191.

45 L. Farrugia, *J. Appl. Crystallogr.*, 1999, **32**, 837–838.

46 M. L. Golden, C. M. Whaley, M. V. Rampersad, J. H. Reibenspies, R. D. Hancock and M. Y. Darensbourg, *Inorg. Chem.*, 2005, **44**, 875–883.

47 G. E. Kenney and A. C. Rosenzweig, *ACS Chem. Biol.*, 2012, 7, 260–268.